ADVANCED OPTICAL MATERIALS
www.advopticalmat.de

www.MaterialsViews.com

Ultracompact Chip-Integrated Electromagnetically Induced Transparency in a Single Plasmonic Composite Nanocavity

Zhen Chai, Xiaoyong Hu, Yu Zhu, Sibai Sun, Hong Yang, and Qihuang Gong**

Electromagnetically-induced transparency (EIT) in plasmonic microstructures originates from the strong destructive interference coupling between ~~wide-band superradiant plasmonic resonances~~ and ~~narrow-band subradiant plasmonic resonances~~. EIT has tremendous potential for application in the fields of nonlinear optics and integrated photonic devices because of its unique ability to reduce the group velocity of light and confine the light into subwavelength-scale regions.[1–3] Various plasmonic microstructure configurations have been adopted to demonstrate EIT, including the use of metamaterials,[4–8] asymmetrically split rings,[9–11] plasmonic resonators,[12,13] and metallic nanoparticle arrays.[14,15] ~~However, the EIT that is realized using these approaches cannot be applied in practical integrated photonic circuits, because the lateral dimensions of the complete plasmonic microstructures are on the order of hundreds of millimeters, and the light signals are illuminated in a direction that is perpendicular to the upper plane of the plasmonic circuits.~~ Chip-integrated EIT structures constructed directly in plasmonic circuits are of particular interest because they can introduce novel functionalities to integrated photonic devices and integrated photonic chips based on plasmonic circuits. Although phase-coupled mechanisms[16,17] and coupled-microcavity mechanisms[18–20] have been presented for construction of chip-integrated EIT structures, very little experimental progress has been made to date. Recently, Han et al. reported a detuned resonator-induced transparency in the near-infrared range using two detuned racetrack resonators that were side-coupled to a bus waveguide etched in a gold film covered by a 300-nm-thick organic polymer layer.[21] However, the diameters of the racetrack plasmonic resonators were as large as 4 μm, which is unsuitable for practical on-chip integration applications.[21] ~~To date, realization of an ultracompact chip-integrated EIT structure in plasmonic circuits remains a considerable challenge.~~

Here, we experimentally demonstrate ultracompact chip-integrated EIT in a single planar plasmonic composite nanocavity in a plasmonic circuit. The plasmonic composite nanocavity consists of two crossed nanogrooves side-coupled to a bus plasmonic waveguide. ~~Wang et al. and Lu et al. have stated that a large (or composite) plasmonic microcavity can sustain multiple plasmonic resonance modes, i.e., microcavity modes.[22,23] Piao et al. noted that a microcavity mode that is strongly coupled to the bus waveguide forms a superradiant mode, while a microcavity mode that is weakly coupled to the bus waveguide forms a subradiant mode.[19]~~ The destructive interference between the two excitation pathways (~~direct excitation of the superradiant microcavity mode, and then excitation of the subradiant microcavity mode through the superradiant microcavity mode~~) was adopted to produce chip-integrated EIT in plasmonic circuits. This is not the only way to obtain EIT (or Fano resonance), because such responses can also be designed based on the deconstruction of plasmonic nanoclusters or the interference between magnetic and electric resonances.[24–26] The lateral dimension of the plasmonic composite nanocavity was only ~~600 nm~~, which is one order of magnitude smaller than that of previously reported structures.[21] In addition, ~~dual-transparency windows~~ were obtained in the near-infrared range and the optical communication range when the plasmonic composite nanocavity was covered with an 80-nm-thick poly(methyl methacrylate) (PMMA) layer. ~~Tunable dual-EIT~~ is attained based on the ~~thermo-optic effect of PMMA~~. This work not only paves the way towards the realization of chip-integrated nanoscale photonic devices, but also opens the possibility of the construction of ultrahigh-speed information processing chips based on plasmonic circuits.

~~The plasmonic composite nanocavity, consisting of two crossed nanogrooves with widths of 150 nm, is side-coupled to a bus plasmonic waveguide etched in a 300-nm-thick gold film, as shown in **Figure 1**(a) and (b).~~ Both the widths and the depths of the two crossed nanogrooves were 150 nm, which were the same as the corresponding values of the bus plasmonic waveguide. The length of the nanogroove in the horizontal direction was 600 nm and that of the nanogroove in the vertical direction was 570 nm. The distance between the nanogroove in the horizontal direction and the bus plasmonic waveguide was 350 nm. The distance between the center of the nanogroove in the horizontal direction and that of the nanogroove in the vertical direction is 140 nm. The bus plasmonic waveguide consists of an air groove with depth of 150 nm and width of 150 nm etched in the gold film. ~~To clarify the propagation properties of the guided surface plasmon polariton (SPP) modes in the plasmonic waveguide used in our experiment, we calculated the power density profile of the SPP mode excited by continuous-wave (CW) incident light at a wavelength of 790 nm using the finite element method,[27] and the calculated profile is shown in Figure 1(c).~~ The guided SPP mode was mainly confined in the nanogroove region, and extended into the upper air region. The maximum intensity was located at the gold/air interface around the two upper corners of the air nanogroove, which agrees well with the calculated results of Li et al.[28]

Dr. Z. Chai, Prof. X. Y. Hu, Dr. Y. Zhu, S. B. Sun, Prof. H. Yang, Prof. Q. H. Gong
State Key Laboratory for Mesoscopic Physics
Department of Physics
Peking University
Beijing 100871, P. R. China
E-mail: xiaoyonghu@pku.edu.cn; qhgong@pku.edu.cn
Prof. X. Y. Hu, Prof. Q. H. Gong
Collaborative Innovation Center of Quantum Matter
Beijing 100871, P. R. China

DOI: 10.1002/adom.201300497

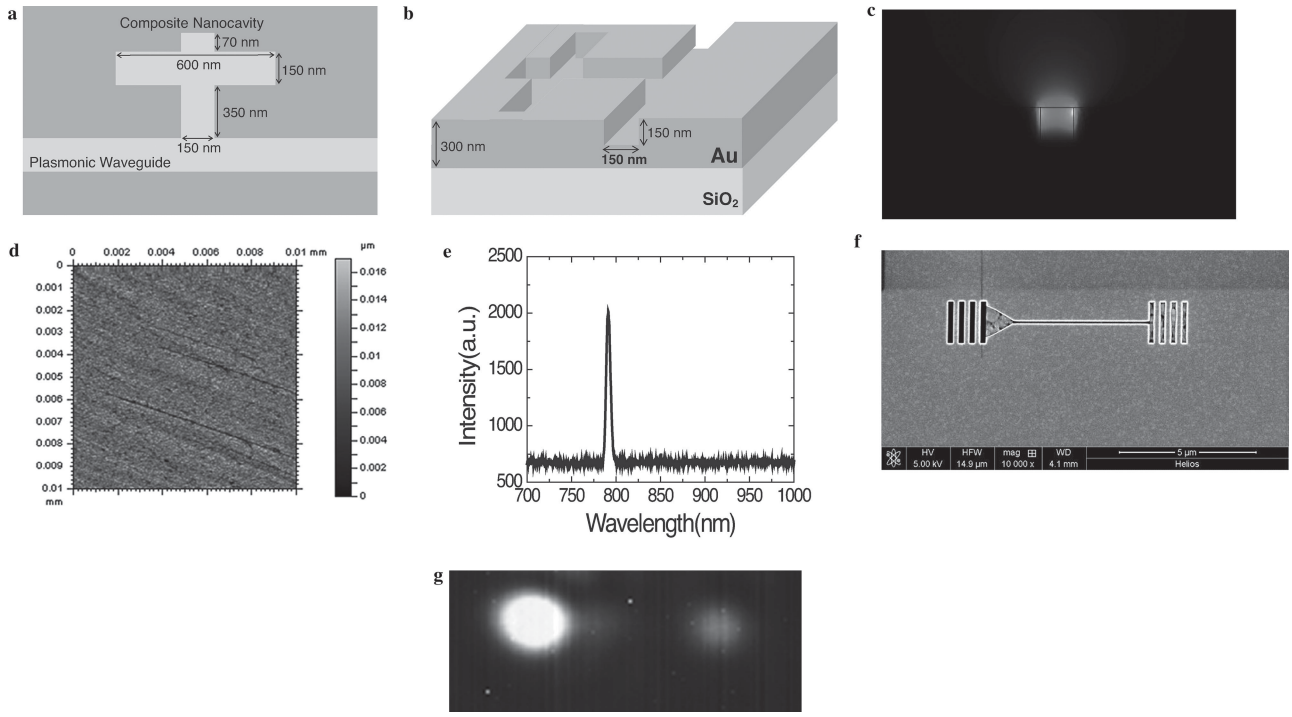

Figure 1. Characterization of the plasmonic composite nanocavity. a) Top-view schematic diagram of the plasmonic composite nanocavity structure. b) Three-dimensional schematic of the structure. c) Power density profile of the SPP mode excited by 790 nm CW incident light. d) AFM image of a 300-nm-thick Au film. e) Laser spectrum of a CW laser beam at a wavelength of 790 nm. f) SEM image of a 7-μm-long straight plasmonic waveguide. g) Measured CCD image of the 7-μm-long straight plasmonic waveguide under excitation by a 790-nm CW laser beam.

The gold film was fabricated using a laser molecular beam epitaxy (LMBE) growth system (Model LMBE 450, SKY Company, China).[29] The beam (with wavelength of 248 nm and pulse width of 25 ns) output from an excimer laser system (Model COMPexPro 205, Coherent Company, USA) was used as the light source. The beam was focused on a gold target mounted on a rotating holder situated 10 mm away from the silicon dioxide substrate. The typical energy density of the laser pulse was 450 mJ/cm^2. The growth rate measured using a film thickness/rate monitor was 0.01 nm/pulse. PMMA powder with an average molecular weight of 10 000 (J&K Company, China) was dissolved in chloroform with a weight ratio of 1:80. Spin coating was used to fabricate 80-nm-thick PMMA layers on the surfaces of the gold films. A high rotational speed of 2000 revolutions per minute was used in our experiment. A focused ion beam etching system (Model Helios NanoLab 600, FEI Company, USA) was used to prepare the plasmonic composite nanocavity patterns. A weak ion beam spot current of only 7.7 pA was used to improve the etching quality. An atomic force microscope (AFM) system (Model MFP-3D, Asylum Company, USA) was used to characterize the quality of the fabricated gold films. An AFM image of a 300-nm-thick gold film is shown in Figure 1(d). The average surface roughness was approximately 8 nm. To effectively excite and collect the required SPPs, we fabricated a coupling grating, with air grooves that were etched through the gold film, connected to a triangular air groove with a depth of 150 nm in the bus plasmonic waveguide input port. A decoupling grating with an air groove depth of 150 nm was also etched in the plasmonic waveguide output port to help couple the SPP mode into free space for measurement purposes. In our experiments, the transmission properties of the plasmonic waveguide were measured using a micro-spectroscopy measurement system.[30] A p-polarized CW Ti:sapphire laser system (Model Mira 900F, Coherent Company, USA) was used as the light source. The spectrum of the laser beam at a wavelength of 790 nm is shown in Figure 1(e). The line width of the laser spectrum curve was only 1.7 nm, which ensures that only the required quasi-monochromatic SPP mode can be excited in the plasmonic waveguide. The coupling grating was normally illuminated from the back side. The optically thick gold film can prohibit direct transmission of the incident laser beam. The SPP mode that propagated through the plasmonic waveguide was scattered using the decoupling grating in the output port. The scattered light was collected using a long working distance objective (Mitutoyo 20, NA = 0.58) and then imaged using a charge coupled device (CCD). To confirm the propagation properties of the guided SPP modes in the plasmonic waveguide, we etched a 7-μm-long straight plasmonic waveguide in a 300-nm-thick gold film, as shown in Figure 1(f). The measured CCD image of the plasmonic waveguide under CW laser beam excitation at a wavelength of 790 nm is shown in Figure 1(g). ~~Remarkable light scattering was obtained using the decoupling grating.~~ The effective refractive index of the plasmonic waveguide for the guided SPP mode excited by the 790 nm CW laser was calculated to be 0.9869–0.009724i, which indicates that the SPP mode propagation length is approximately 6.5 μm. This evidence confirms the perfect waveguiding properties of the plasmonic waveguide.

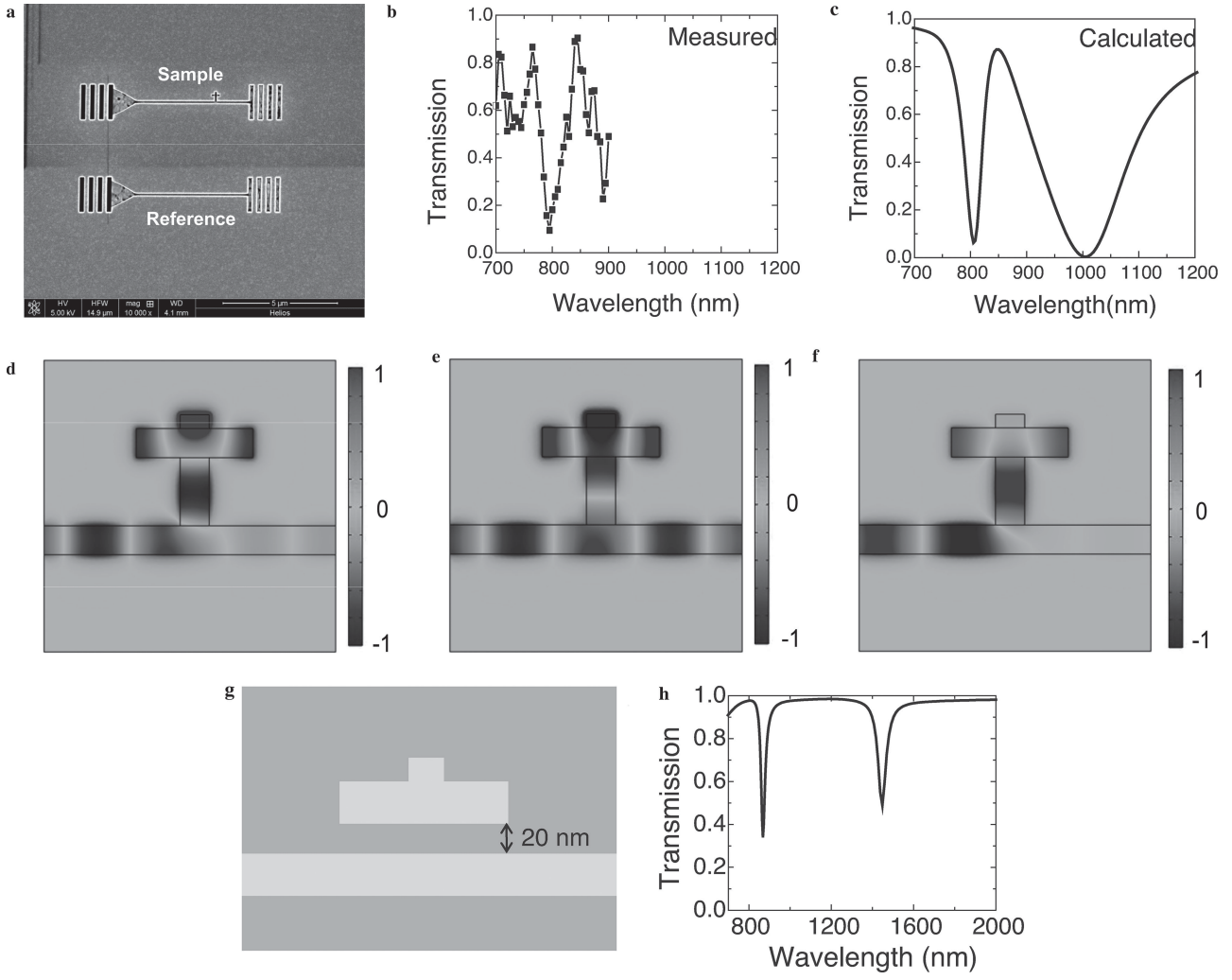

Figure 2. a) SEM image of the plasmonic composite nanocavity. Measured b) and calculated c) transmission spectra of the plasmonic composite nanocavity. Calculated magnetic field distributions of the plasmonic composite nanocavity under excitation by CW incident light at wavelengths of d) 800 nm, e) 850 nm, and f) 1000 nm. g) Schematic of the plasmonic composite nanocavity structure without the lower vertical cavity. h) Calculated transmission spectrum of the plasmonic composite nanocavity without the lower vertical cavity.

To study the transmission properties of the plasmonic composite nanocavity, as shown in **Figure 2**(a), we measured the transmission spectrum of the bus plasmonic waveguide that is side-coupled to the plasmonic composite nanocavity, and the measured results are shown in Figure 2(b). The ~~linear transmission~~ was normalized with respect to a reference straight plasmonic waveguide, as shown in Figure 2(a), which is the standard method used to study the linear transmission properties of plasmonic microcavities.[21] The spot size of the incident laser beam was 8 μm, which ensures nearly-equal average excitation intensities for the coupling gratings of both the composite nanocavity sample and the reference waveguide. The limits of the tunable wavelength range of the Ti:sapphire laser system meant that we could only measure the transmission spectrum from 700 to 900 nm. In the measured transmission spectrum, a sharp and high transmission peak appeared in the transmission forbidden band, which implies EIT formation. The plasmonic composite nanocavity provides multiple microcavity modes, which was confirmed by the calculations of Wang et al. and Lu et al.[22,23] The microcavity mode related to the vertical nanogroove of the composite nanocavity can be excited very easily by the SPPs propagating in the bus waveguide to form the superradiant mode. Howeve, the microcavity mode related to the horizontal nanogroove of the composite nanocavity is difficult to excite directly with the SPPs propagating in the bus waveguide, and this has been confirmed by the calculations of Piao et al.[19] The destructive interference between the two excitation pathways, i.e., direct excitation of the superradiant microcavity mode, and excitation of the subradiant mode through the superradiant microcavity mode, forms the EIT effect. The central wavelength and the peak transmission of the transparency window were 850 nm and 90%, respectively, which is in good agreement with the values calculated using the finite element method, as shown in Figure 2(c). To further confirm the measured results, we also used the finite element method to calculate the magnetic field distribution of the plasmonic composite nanocavity under excitation by CW incident light at wavelengths of 800 nm (located at the

transmission minimum in the short-wavelength direction), 850 nm (located at the center of the transparency window), and 1000 nm (located at the transmission minimum in the long-wavelength direction), and the calculated results are shown in Figure 2(d–f). For the incident light at wavelengths of 800 and 1000 nm, the magnetic field distribution was mainly confined within the vertical nanogroove of the plasmonic composite nanocavity, as shown in Figure 2(d,f). This indicates that the microcavity modes related to the vertical nanogroove form the superradiant mode. For the incident light at the wavelength of 850 nm, the magnetic field distribution was mainly confined within the horizontal nanogroove of the plasmonic composite nanocavity, as shown in Figure 2(e), which indicates that the microcavity mode related to the horizontal nanogroove forms the subradiant mode. To further confirm our measured results, we also calculated the transmission spectrum of the bus plasmonic waveguide when side-coupled to a nanocavity consisting of the horizontal nanogroove connected to the upper part of the vertical nanogroove (as shown in Figure 2(g)), and the calculated results are shown in Figure 2(h). The distance between the horizontal nanogroove and the bus waveguide was set to be 20 nm to enable easy excitation of the microcavity modes. The other structural parameters were the same as those of the plasmonic composite nanocavity. There is a microcavity mode with a resonant wavelength at around 850 nm, as shown in Figure 2(h). This confirms that ultracompact chip-integrated EIT is realized based on the two different excitation pathways related to the superradiant and subradiant microcavity modes.

To study the EIT tunability, we used the finite element method to calculate the transmission spectrum of the bus waveguide side-coupled to the plasmonic composite nanocavity covered with an 80-nm-thick PMMA layer, and the calculated results are as shown in **Figure 3**(a). The refractive index of PMMA was set to be 1.49. The center of the transparency window shifted in the long-wavelength direction when the plasmonic composite nanocavity was covered with the 80-nm-thick PMMA layer. The resonant mode of the plasmonic resonator is influenced enormously by the refractive index of the ambient dielectric material. The refractive index of the ambient dielectric material increases when the plasmonic composite nanocavity is covered by the PMMA layer, which leads to a red-shift in the resonant wavelength of the microcavity modes.[31] The central wavelength of the transparency window shifts accordingly in the long-wavelength direction. The central wavelength of the transparency window changed from 850 nm to 1340 nm when the ambient dielectric material changed from air to PMMA. A 490 nm shift in the central wavelength of the transparency window was thus obtained. To confirm the calculated results, we measured the transmission of the bus waveguide that was side-coupled to the plasmonic composite nanocavity covered with an 80-nm-thick PMMA layer. Our measurements show that the PMMA cover layer was very flat and uniform on top of the sample. The strong surface tension related to the small widths of the air nanogrooves and the high rotational speed of 2000 revolutions per minute ensure the formation of the flat and uniform PMMA cover layer. Limited by the available experimental conditions in our laboratory, we only measured the transmission of the bus waveguide at wavelengths of 1340 nm (located at the center of the transparency window) and 1580 nm (located at a transmission minimum) using a homemade CW laser system, and the measured results are as shown in Figure 3(a). High transmission of 87% was obtained at 1340 nm, while a small transmission of 7% was achieved at 1580 nm, which is in good agreement with the calculated values, as shown in Figure 3(a). Figure 3(b) shows the measured CCD images of the composite nanocavity sample and the reference waveguide, covered with the 80-nm-thick PMMA layer, under excitation by a CW incident laser at a wavelength of 1340 nm. Strong scattered light was obtained from the decoupling gratings of both the plasmonic composite nanocavity sample and the reference waveguide. This indicates that the guided SPP mode can propagate through the composite nanocavity under

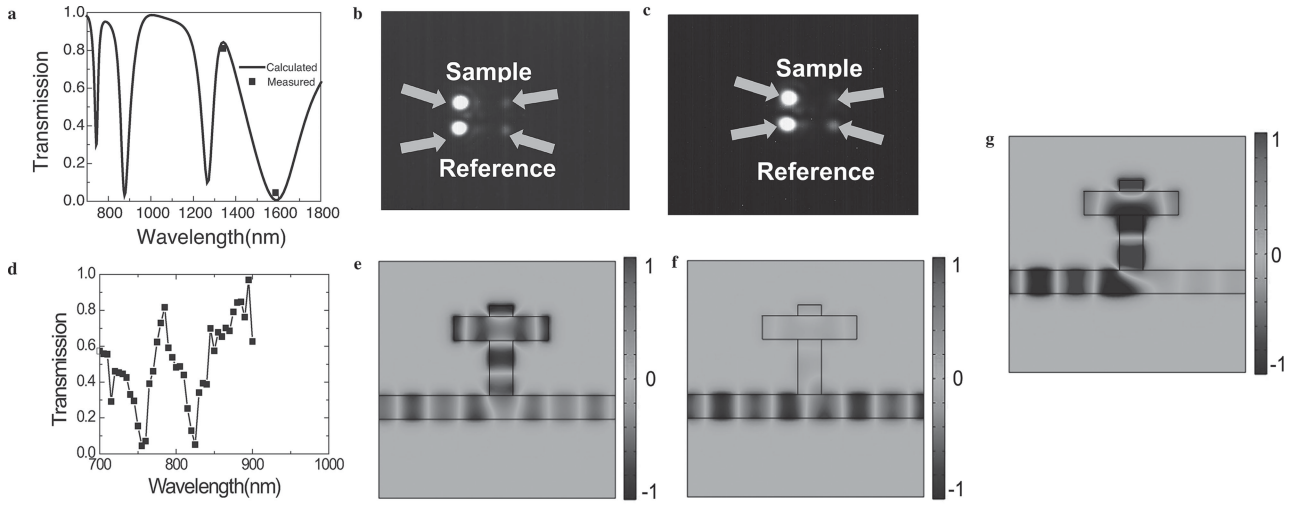

Figure 3. a) Transmission spectrum of the plasmonic composite nanocavity covered with an 80-nm-thick PMMA layer. Measured CCD images of the plasmonic composite nanocavity sample and the reference plasmonic waveguide, covered by the 80-nm-thick PMMA layer, under CW incident laser excitation at wavelengths of b) 1340 nm and c) 1580 nm. d) Measured transmission spectrum from 700 to 900 nm of the plasmonic composite nanocavity covered by the 80-nm-thick PMMA layer. Calculated magnetic field distributions of the plasmonic composite nanocavity under CW light excitation at wavelengths of e) 740 nm, f) 780 nm, and g) 870 nm.

the excitation of the 1340 nm incident laser. Figure 3(c) shows the measured CCD images of the composite nanocavity sample and the reference waveguide, covered with the 80-nm-thick PMMA layer, under excitation by a CW incident laser at a wavelength of 1580 nm. Very weak scattered light was obtained from the decoupling grating of the plasmonic composite nanocavity in this case, while strong scattered light was obtained from the decoupling grating of the reference waveguide. This indicates that the guided SPP mode can not propagate through the composite nanocavity under excitation by a 1580 nm laser. This confirms that the perfect EIT effect has been obtained. We also measured the transmission spectrum of the bus waveguide that was side-coupled to the plasmonic composite nanocavity covered with the 80-nm-thick PMMA layer from 700 to 900 nm, and the measured results are as shown in Figure 3(d). A sharp and high transmission peak appeared in the transmission forbidden band, which implies the formation of an EIT-like effect. The central wavelength and the peak transmission of the transparency window were 780 nm and 85%, respectively, which shows good agreement with the calculated values, as shown in Figure 3(a). To confirm the measured results, we calculated themagnetic field distribution of the composite nanocavity covered with the 80-nm-thick PMMA layer under excitation by CW incident light at wavelengths of 740 nm (located at the transmission minimum in the short-wavelength direction), 780 nm (located in the center of the transparency window), and 870 nm (located at the transmission minimum in the long-wavelength direction) using the finite element method, and the calculated results are as shown in ~~Figure 3(e) to (g)~~. For the incident light at wavelengths of 740 and 870 nm, the magnetic field distribution was mainly confined within the plasmonic composite nanocavity, as shown in Figure 3(e) and (g). This indicates that the transmission minimum originates from the microcavity modes of the composite nanocavity. For the incident light at the wavelength of 780 nm, the magnetic field distribution was mainly confined within the bus waveguide, as shown in Figure 3(f), which indicates that the transmission maximum originates from the guided SPP mode of the bus waveguide, which is not resonant with the plasmonic composite nanocavity. This confirms that the sharp transmission peak is caused by an EIT-like effect. Therefore, dual transparency windows are obtained when the plasmonic composite nanocavity is covered with the 80-nm-thick PMMA layer. To study the thermal tunability of this dual EIT, we calculated the transmission spectrum of the plasmonic composite nanocavity covered with an 80-nm-thick PMMA layer at different ambient temperatures by the finite element method, and the calculated results are as shown in **Figure 4.** The central wavelengths of the two transparency windows shifted in the short-wavelength direction with increasing ambient temperature. PMMA has a negative value for the thermo-optic coefficient dn/dT of -1.2×10^{-4} °C^{-1}.[32] The refractive index of PMMA decreases with increasing ambient temperature, which results in a blue-shift in the resonant wavelengths of the microcavity modes of the plasmonic composite nanocavity.[31] As a result, the central wavelengths of the two transparency windows shifted in the short-wavelength direction. When the ambient temperature rose from 25 to 80 °C, the central wavelength of the transparency window in the optical communication range varied from 1340 to 1270 nm, spanning a 70 nm range; while the central wavelengths of the transparency window in the near infrared range varied from 780 to 740 nm, spanning a 40 nm range. In addition, the response time of the thermo-optic effect of PMMA was of the order of several microseconds.[32] Therefore, fast thermally-tunable dual EIT with a wide tunability range can be realized.

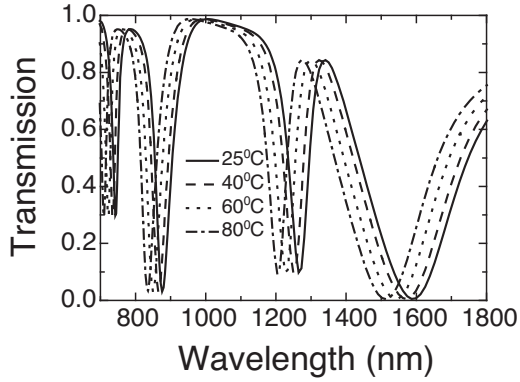

Figure 4. Calculated transmission spectrum of the plasmonic composite nanocavity covered with an 80-nm-thick PMMA layer at different ambient temperatures.

In conclusion, we have experimentally realized ultracompact chip-integrated EIT in a single composite nanocavity in a plasmonic circuit. A small lateral dimension of 600 nm was obtained. A large shift in the central wavelength of the transparency window of 490 nm was obtained when the composite nanocavity was coated with a PMMA layer. An additional EIT-like effect was obtained in the near-infrared range. This work paves the way for construction of nanoscale photonic devices and integrated photonic chips.

Acknowledgements

This work was supported by the 973 Program of China under grant nos. 2013CB328704 and 2014CB921003, the National Natural Science Foundation of China under grant nos. 11225417, 11134001, 11121091, and 90921008, and the Program for NCET in University.

Received: November 28, 2013
Revised: January 17, 2014
Published online: February 6, 2014

[1] B. Luk'yanchuk, N. I. Zheludev, S. A. Maier, N. J. Halas, P. Nordlander, H. Giessen, C. T. Chong, *Nature Mater.* **2010**, *9*, 707.
[2] M. Rahmani, B. Luk'yanchuk, M. H. Hong, *Laser Photon. Rev.* **2013**, *7*, 329.
[3] N. Liu, M. Hentschel, T. Weiss, A. P. Alivisatos, H. Giessen, *Science* **2011**, *332*, 1407.
[4] C. Kurter, P. Tassin, L. Zhang, T. Koschny, A. P. Zhuravel, A. V. Ustinov, S. M. Anlage, C. M. Soukoulis, *Phys. Rev. Lett.* **2011**, *107*, 043901.
[5] P. Tassin, L. Zhang, T. Koschny, E. N. Economou, C. M. Soukoulis, *Phys. Rev. Lett.* **2009**, *102*, 053901.
[6] N. Papasimakis, V. A. Fedotov, N. I. Zheludev, S. L. Prosvirnin, *Phys. Rev. Lett.* **2008**, *101*, 253903.

[7] S. Zhang, D. A. Genov, Y. Wang, M. Liu, X. Zhang, *Phys. Rev. Lett.* **2008**, *101*, 047401.
[8] S. Y. Chiam, R. Singh, C. Rockstuhl, F. Lederer, W. Zhang, A. A. Bettiol, *Phys. Rev. Lett.* **2009**, *80*, 153103.
[9] J. Q. Gu, R. Singh, X. J. Liu, X. Q. Zhang, Y. F. Ma, S. Zhang, S. A. Maier, Z. Tian, A. K. Azad, H. T. Chen, A. J. Taylor, J. G. Han, W. L. Zhang, *Nature Commun.* **2012**, *3*, 1151.
[10] X. Q. Lin, J. W. Yu, Y. Jiang, J. Y. Jin, Y. Fan, *Appl. Phys. Lett.* **2012**, *101*, 093502.
[11] Q. Bai, C. Liu, J. Chen, C. Cheng, M. Kang, H. T. Wang, *J. Appl. Phys.* **2010**, *107*, 093104.
[12] N. Verellen, Y. Sonnefraud, H. Sobhani, F. Hao, V. V. Moshchalkov, P. V. Dorpe, P. Nordlander, S. A. Maier, *Nano Lett.* **2009**, *9*, 1663.
[13] T. Zentgraf, S. Zhang, R. F. Oulton, X. Zhang, *Phys. Rev. B* **2009**, *80*, 195415.
[14] V. Yannopapas, E. Paspalakis, N. V. Vitanov, *Phys.Rev. B* **2009**, *80*, 035104.
[15] C. Rohde, K. Hasegawa, M. Deutsch, *Opt. Lett.* **2007**, *32*, 415.
[16] R. D. Kekatpure, E. S. Barnard, W. Cai, M. L. Brongersma, *Phys. Rev. Lett.* **2010**, *104*, 243902.
[17] J. J. Chen, C. Wang, R. Zhang, J. H. Xiao, *Opt. Lett.* **2012**, *37*, 5133.
[18] Z. H. Han, S. I. Bozhevolnyi, *Opt. Express* **2011**, *19*, 3251.
[19] X. Piao, S. Yu, N. Park, *Opt. Express* **2012**, *20*, 18994.
[20] H. Lu, X. M. Liu, D. Mao, Y. K. Gong, G. X. Wang, *Opt. Lett.* **2011**, *36*, 3233.
[21] Z. H. Han, C. E. G. Ortiz, I. P. Radko, S. I. Bozhevolnyi, *Opt. Lett.* **2013**, *36*, 875.
[22] T. B. Wang, X. W. Wen, C. P. Yin, H. Z. Wang, *Opt. Express* **2009**, *17*, 24096.
[23] H. Lu, X. M. Liu, D. Mao, L. Wang, Y. K. Gong, *Opt. Express* **2010**, *18*, 17922.
[24] J. B. Lassiter, H. Sobhani, M. W. Knight, W. S. Mielczarek, P. Nordlander, N. J. Halas, *Nano Lett.* **2012**, *12*, 1058.
[25] M. Rahmani, D. Y. Lei, V. Giannini, B. Lukiyanchuk, M. Ranjbar, T. Y. F. Liew, M. H. Hong, S. A. Maier, *Nano Lett.* **2012**, *12*, 2101.
[26] J. Yang, M. Rahmani, J. H. Teng, M. H. Hong, *Opt. Mater. Express* **2012**, *2*, 1407.
[27] Z. Chai, X. Y. Hu, Y. Zhu, F. Zhang, H. Yang, Q. H. Gong, *Appl. Phys. Lett.* **2013**, *102*, 201119.
[28] X. E. Li, T. Jiang, L. F. Shen, X. H. Deng, *Appl. Phys. Lett.* **2013**, *102*, 031606.
[29] Y. Zhu, X. Y. Hu, Y. Y. Huang, H. Yang, Q. H. Gong, *Adv. Optical Mater.* **2013**, *1*, 61.
[30] Y. L. Fu, X. Y. Hu, C. C. Lu, S. Yue, H. Yang, Q. H. Gong, *Nano Lett.* **2012**, *12*, 5784.
[31] P. Mulvaney, *Langmuir* **1996**, *12*, 788.
[32] M. B. J. Diemeer, J. J. Brons, E. S. Trommel, *J. Lightwave Technol.* **1997**, *7*, 449.